RSC Advances

$LiTi_2(PO_4)_3$/reduced graphene oxide nanocomposite with enhanced electrochemical performance for lithium-ion batteries

Journal:	*RSC Advances*
Manuscript ID:	RA-ART-05-2014-004943.R1
Article Type:	Paper
Date Submitted by the Author:	05-Jul-2014
Complete List of Authors:	Roh, Ha-kyung; Yonsei University, Department of Material Science and Engineering Kim, Hyun-Kyung; Yonsei University, Department of Material Science and Engineering Roh, Kwang Chul; Korea Institute of Ceramic Engineering & Technology, Energy & Environmental Division Kim, Kwang Bum; Yonsei University, Department of Material Science and Engineering

RSC advances

RSCPublishing

ARTICLE

$LiTi_2(PO_4)_3$/reduced graphene oxide nanocomposite with enhanced electrochemical performance for lithium-ion batteries

Cite this: DOI: 10.1039/x0xx00000x

Received 00th January 2012,
Accepted 00th January 2012

DOI: 10.1039/x0xx00000x

www.rsc.org/

Ha-Kyung Roh,[a] Hyun-Kyung Kim,[a] Kwang Chul Roh,[*b] and Kwang-Bum Kim[*a]

An $LiTi_2(PO_4)_3$/reduced graphene oxide (rGO) nanocomposite with a NASICON-type structure was synthesized using a simple microwave-assisted one-pot method followed by calcination. The $LiTi_2(PO_4)_3$ nanoparticles were uniformly deposited on rGO substrates, and the size of $LiTi_2(PO_4)_3$ particles in the composite was 30–40 nm. Electrodes prepared from the nanocomposite delivered a reversible capacity of 138 mAh g^{-1} at a 0.1 C-rate and apparent diffusion coefficient of Li^+ in the anode, as calculated from the cyclic voltammetry curves, is 1.55×10^{-14} cm^2 s^{-1}. The electrode exhibited good charge/discharge cycling stability, retaining over 93.2 % of its initial capacity after 100 cycles at 1 C-rate and reaching a coulombic efficiency of approximately 99.8 %. This excellent cycle stability is further confirmed by TEM analysis, which reveals that almost all of the $LiTi_2(PO_4)_3$ nanoparticles remain unchanged after 200 cycles.

Introduction

With the rapid growth in the use of portable electronics and power electric vehicles (EVs), high-performance energy storage systems are in great demand.[1, 2] Lithium-ion battery (LIB) has attracted considerable attention as one of the most capable power sources because of the highest energy density among any rechargeable batteries, as well as good power density and cycle life.[3-5] At present, various forms of graphitic carbon are used as anode materials in LIBs. However, these materials have drawbacks such as poor cyclability and high reactivity with electrolyte solutions.[6-8] For these reasons, the search for new electrode materials that possess improved electrochemical performance and safety has become paramount.[9, 10]

NASICON-structured $LiTi_2(PO_4)_3$ is considered an outstanding potential anode material for LIBs because of the rapid Li^+ diffusion in the bulk and on surface of $LiTi_2(PO_4)_3$.[11-15] $LiTi_2(PO_4)_3$ can reversibly accommodate two additional lithium ions, operating on the Ti^{4+}/Ti^{3+} at 2.48 V, *via* a two-phase mechanism that converts between $LiTi_2(PO_4)_3$ and $Li_3Ti_2(PO_4)_3$. The crystal structure of $LiTi_2(PO_4)_3$ is a three dimensional network in which TiO_6 octahedra share all their corners with PO_4 tetrahedra. The interstitial and conduction channels are aligned along the c-axis, and the Li^+ can be found occupying interstitial sites, thus it can move easily along the conduction channels.[11] In addition, in this structure, the $LiTi_2(PO_4)_3$ framework is well preserved during Li^+ extraction.[16] The phase transformations are mainly due to the Li^+ re-ordering in different sites, not causing changes in the lattice framework so that it leads to long cycle life and safety performance. Despite these advantages, $LiTi_2(PO_4)_3$ suffers from intrinsically poor electronic conductivity (10^{-8} S cm^{-1}), which leads to poor charging/discharging rate performance of LIBs.

Various approaches for improving the rate capability and cycling performance, such as the reduction of particle size, the addition of a surface coating[11, 13, 14] and the synthesis of composite materials with conductive carbons[12, 17] have been applied. For example, Luo *et al.*[11] reported the synthesis of $LiTi_2(PO_4)_3$ using a sol-gel method followed by 12 wt.% carbon-coating which provided a discharge capacity of 130 mAh g^{-1} at 0.1 C between 1.5 and 3.5 V *vs.* Li^+/Li. Wessells *et al.*[15] reported the electrochemical properties of 4 wt.% carbon-coated $LiTi_2(PO_4)_3$ synthesized using Pechini's method with discharge capacities of ~115 and ~96.6 mAh g^{-1} at the first cycle and after 100 cycles, respectively, between 2.0 and 3.0 V *vs.* Li at 1 C-rate. Zhou *et al.*[17] reported the synthesis of $LiTi_2(PO_4)_3$/acetylene black nanocomposites using a polyvinyl acetate (PVA) assisted sol-gel method, which showed a discharge capacity of 129.4 mAh g^{-1} at 0.1 C-rate between 1.5 and 3.5 V *vs.* Li. To examine the behavior of carbon additives, they prepared the pure-$LiTi_2(PO_4)_3$ and $LiTi_2(PO_4)_3$/C samples. The initial discharge capacities of both pure-$LiTi_2(PO_4)_3$ and $LiTi_2(PO_4)_3$/C are 90.3 and 112.8 mAh g^{-1} at 0.5 C-rate, respectively. In summary, structuring $LiTi_2(PO_4)_3$ at the nano-scale typically increases the effective interfacial area between the active also material and the electrolyte. Furthermore, a

smaller particle size helps shorten the lithium-ion diffusion path, thereby improving the electrochemical utilization of $LiTi_2(PO_4)_3$ at high discharge/charge rates that increases the overall capacity. Additionally, hybridization with conductive carbonaceous materials improves the electronic conductivity of the nanostructured electrodes and enhances the rate capability.

Among the carbonaceous electrode materials available, graphene and reduced graphene oxide (rGO) have great potential as electroactive materials and conductive agents in energy storage applications given their high surface-to-volume ratio, superior electron transport, and excellent mechanical properties.[18-21] Electrically conductive rGO flakes can not only be used as a conductive template for metal oxide precipitate in the synthesis of metal oxide nanoparticle/rGO composites but can also effectively prevent the agglomeration of nanoparticles into larger particles during the charge/discharge cycling process.[22-24] In addition, the nucleation and growth of metal oxides on rGO templates can effectively reduce restacking of the graphene flakes, maintaining their high active surface areas. This improves the electrochemical utilization of oxide nanoparticles, and thus metal oxide nanoparticle/rGO composite materials provide much better rate capabilities than other types of composites.

Although some metal oxide/rGO composites (e.g., CuO/, NiO/, Mn_3O_4/, Co_3O_4/, Fe_2O_3/rGO) have been synthesized,[25-29] to the best of our knowledge, only a few studies have investigated the synthesis of $LiTi_2(PO_4)_3$/rGO composites.[30] Most recently, Kim's group reported the synthesis of an $LiTi_2(PO_4)_3$/rGO composite using a solid-state method with rGO as a conducting reinforcement. This composite exhibited a capacity retention of 85 % after 200 cycles at 5 C-rate between 1.5 and 3.5 V *vs.* Li, however, it is still challenging to improve the cyclability.[30] Additionally, their synthesis of the $LiTi_2(PO_4)_3$/rGO composite was a traditional two-step procedure consisting of first the formation of a TiO_2-GO hybrid material, and a subsequent lithiation stage to form the Li–Ti–P–O/rGO hybrid. Finally, this product was heated to form the NASICON-structured $LiTi_2(PO_4)_3$/rGO composite. In this two-step method, however, the lithiation and heat treatment steps unfavorably affect the size, morphology, and homogeneity of the resulting $LiTi_2(PO_4)_3$ particles. Moreover, the complicated and time-consuming nature of this two-step approach results in an inhomogeneous dispersion of nanoparticles on the rGO surface.

Here, we report a simple one-pot synthesis of $LiTi_2(PO_4)_3$/rGO nanocomposites *via* a microwave-assisted solvothermal method that combines the advantages of simplicity and efficiency. Electrodes prepared from the nanocomposites provide excellent cycling performance and rate capability, indicating great potential for their use in LIBs.

Experimental

The $LiTi_2(PO_4)_3$/rGO nanocomposite was synthesized from an Li–Ti–P–O/rGO intermediate precursor *via* a microwave-assisted solvothermal method using one-pot and subsequent heat treatment. GO flakes (100 mg), prepared using the modified Hummers' method,[31] were dispersed in 100 ml of diethyleneglycol (DEG) with sonication for 30 min, then 0.42 ml of $Ti(OC_2H_5)_4$ was added to the above dispersion under stirring. 40 ml of this solution was loaded into each of two Teflon vessels, after which 5 ml of 2 M LiOH solution and 4 ml of 3 M $NH_4H_2(PO_4)_3$ solution were added. The resulting mixtures were treated in a microwave oven (MARS, CEM Corp.), the reaction product was washed with ethanol and distilled water several times, and then freeze-dried for 24 h. The resulting Li–Ti–P–O/rGO precursor was calcined under an argon gas atmosphere at 800 °C for 10 h to obtain a well-crystallized $LiTi_2(PO_4)_3$/rGO nanocomposite. Additionally, "bare" $LiTi_2(PO_4)_3$, without rGO or any carbonaceous materials, was prepared using the conventional Pechini method[32] for comparison purposes as shown in Fig. S1.†

The crystalline phases, structures and the morphology of the materials were characterized by X-ray diffractometer (XRD) using a Rigaku D/max 2200V/PC with Cu Kα radiation (λ = 1.54178Å), high-resolution transmission electron microscopy (HR-TEM) using a FEI Tecnai F20 at 200kV, and Raman spectrometry using a Jobin Yvon-Spex, LABram. X-ray photoelectron spectrometry (XPS) using a Thermo Electron Corporation ESCA Lab 250 at 15 kV and 150 W was employed to analyze the degree of reduction of the graphene oxide. To estimate the loading of $LiTi_2(PO_4)_3$ in the composite, elemental analysis (2400 Series II, PerkinElmer) and a thermogravimetric analysis (TGA, Bruker TGA-DTA2010SA) was performed.

The electrochemical experiments were performed using a CR2032 coin cell incorporating a metallic lithium foil counter electrode. The working electrode was prepared from a mixture of 90 wt.% $LiTi_2(PO_4)_3$/rGO nanocomposite, 5 wt.% carbon black as a conductive additive, and 5 wt.% polyvinylidene fluoride dissolved in N-methylpyrrolidone as a binder. This slurry was spread onto copper foil and then dried at 100 °C for 12 h. The loading of dried slurry was 2–3 mg cm^{-2} for each working electrode. 1 M $LiPF_6$ was dissolved in a mixture of ethyl carbonate and dimethyl carbonate in a volume ratio of 1:1 and used as the electrolyte.

Galvanostatic charge/discharge tests, cyclic voltammetry (CV), and electrochemical impedance spectroscopy (EIS) were conducted using a Princeton Applied Research VMP2 potentiostat/galvanostat. CV was performed at scan rates ranging from 0.1 to 5 mV s^{-1} in a potential window of 2.0–3.0 V *vs.* Li^+/Li. The EIS measurements were performed at room temperature after three charge/discharge cycles and subsequently conducted at 2.46 V vs. Li^+/Li with a 5 mV voltage amplitude over frequencies ranging from 100 kHz to 10 mHz.

Results and discussion

Scheme. 1 illustrates the microwave-assisted synthesis of the $LiTi_2(PO_4)_3$/rGO nanocomposite. First, an Li–Ti–P–O intermediate precursor is formed *in-situ* on partially reduced GO from a mixed solution of GO, titanium, phosphate, and

lithium precursors in a microwave-assisted process. This microwave-assisted solvothermal approach offers several advantages compared to the conventional solvothermal methods.[33] The dielectric microwave heating leads to direct interactions between the microwaves and reactants inside the sealed reaction vessel, which reduces the reaction time and provides energy savings.[34-36] Moreover, the conductive rGO template absorbs microwaves and is selectively heated within a short period of time under microwave irradiation, resulting in a higher temperature on the rGO surface than in diethylene glycol solution. This facilitates the heterogeneous nucleation and growth of the precipitates on the surface of rGO rather than the homogeneous nucleation and growth in the bulk solution, so that extremely small Li–Ti–P–O precursor particles can be uniformly decorated on the surface of the rGO substrate.[37, 38] Finally, after calcination at 800 °C, the $LiTi_2(PO_4)_3$/rGO nanocomposites were synthesized as final products, during which the Li–Ti–P–O/rGO intermediate precursor could be completely transformed into well-crystallized $LiTi_2(PO_4)_3$/rGO nanocomposite without morphological changes.

Powder X-ray diffractometry (XRD) results for both the Li–Ti–P–O/rGO intermediate precursor and the $LiTi_2(PO_4)_3$/rGO nanocomposite are shown in Fig. 1(a). The XRD pattern of the Li–Ti–P–O/rGO intermediate precursor indicated the formation of an amorphous phase. When calcined at 800 °C under an argon atmosphere, the amorphous Li–Ti–P–O/rGO precursor could be completely converted into the crystalline $LiTi_2(PO_4)_3$/rGO nanocomposite; this is consistent with the Raman data (Fig. S3†). The major characteristic peaks of (012), (104), (113), (202), (024), (211), (116) and (300) from $LiTi_2(PO_4)_3$/rGO composites, unlike those of the amorphous Li–Ti–P–O/rGO, could be indexed to the rhombohedral NASICON-type structure with a space group of R3C (JCPDS 35-0754). A broad (002) reflection appearing over a 2θ range of 25–27° corresponds to the formation of the rGO flakes. All of these diffraction peaks are strong and narrow, indicating highly crystalline $LiTi_2(PO_4)_3$.

The morphology and structural features of $LiTi_2(PO_4)_3$/rGO composite were observed by high-resolution TEM (HR-TEM) and field-emission SEM (FE-SEM). As shown in Figs. 1(b) and (c), $LiTi_2(PO_4)_3$ nanoparticles with a narrow size distribution in the range of 30–40 nm are uniformly decorated on the rGO template, which prevents the agglomeration of individual $LiTi_2(PO_4)_3$ nanoparticles.

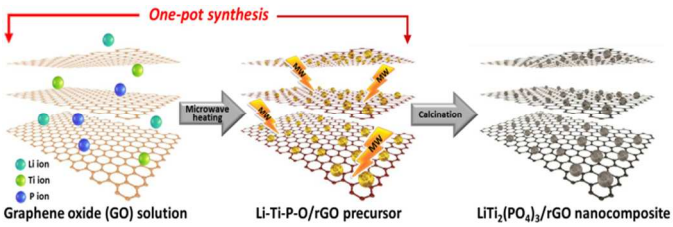

Scheme. 1 Schematic illustration of the fabrication of the $LiTi_2(PO_4)_3$/rGO nanocomposite from a precursor using the microwave-assisted one-pot method.

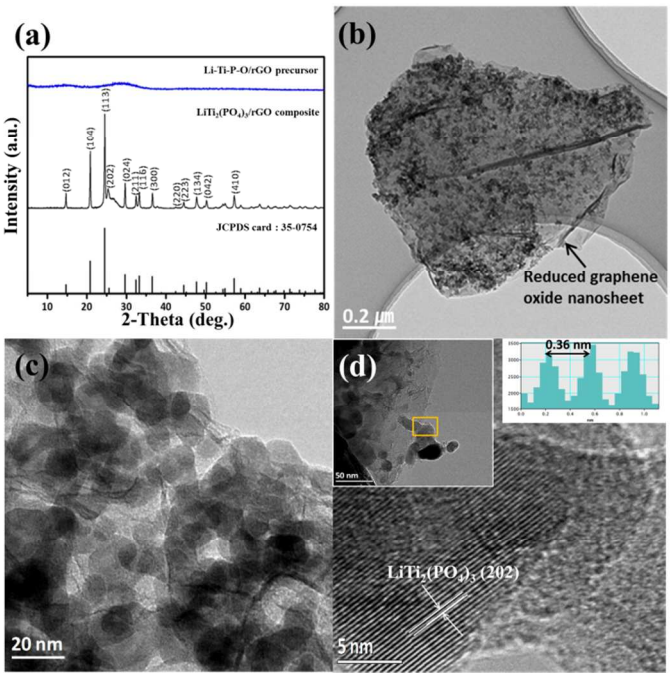

Fig. 1 (a) XRD patterns of Li-Ti-P-O/rGO intermediate precursor, the $LiTi_2(PO_4)_3$/rGO nanocomposite, and the NASICON-structured $LiTi_2(PO_4)_3$ (JCPDS No.35-0754). (b), (c) TEM images of uniformly dispersed $LiTi_2(PO_4)_3$ particles on rGO sheets with particle sizes of 30–40 nm. (d) HR-TEM images of the well-crystallized $LiTi_2(PO_4)_3$/rGO.

During the calcination heat treatment to transform the Li–Ti–P–O/rGO intermediate precursor into the $LiTi_2(PO_4)_3$/rGO nanocomposite, particle size growth or morphological changes were not observed as determined by TEM and SEM (Fig. S2†). The clear lattice fringes observed in the HR-TEM image in Fig. 1(d) demonstrate the high crystallinity of the $LiTi_2(PO_4)_3$ nanoparticles in the composite, which is consistent with the XRD results. The lattice parameter (a_0) of the NASICON-structured $LiTi_2(PO_4)_3$ is 0.36 nm, as shown in the inset of Fig. 1(d). This is consistent with the *d*-spacing of the (202) planes calculated based on the diffraction angle using Bragg's law.

The $LiTi_2(PO_4)_3$/rGO nanocomposite was further characterized by X-ray photoelectron spectroscopy (XPS), and the spectrum was analyzed using the Gaussian fitting method. As shown in Fig. 2(a), the elements present were Ti, P, O, and C, as expected for an $LiTi_2(PO_4)_3$/rGO composite. The Ti 2*p*, P 2*p* and O 1*s* XPS signatures confirm the presence of $LiTi_2(PO_4)_3$. The expanded C 1*s* regions shown in Figs. 2(b)–(d) indicate a degree of reduction of the GO, with four components corresponding to carbon atoms in different functional groups: C–C, C–O, C=O and O–C=O. It is clearly seen that the peak at 284.7 eV (C–C) for the $LiTi_2(PO_4)_3$/rGO composite peak at [Fig. 2(d)] increased, while the peaks at 286.2 eV (C–O), 287.7 eV (C=O), and 290.3 eV (O–C=O) decreased drastically after calcination. The intensities associated with these oxygen-bearing functional groups were reduced substantially in the composite as compared to the GO and Li–Ti–P–O/rGO intermediate, indicating the complete reduction of GO to rGO.

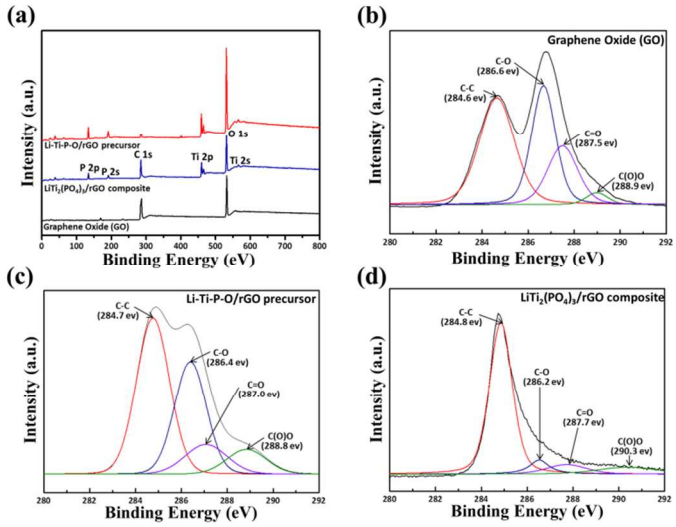

Fig. 2 (a) XPS data for GO, the Li-Ti-P-O/partially reduced GO precursor, and the $LiTi_2(PO_4)_3$/rGO composite; the C 1*s* regions of the spectra for each of these materials are shown expanded in (b) , (c), and (d), respectively.

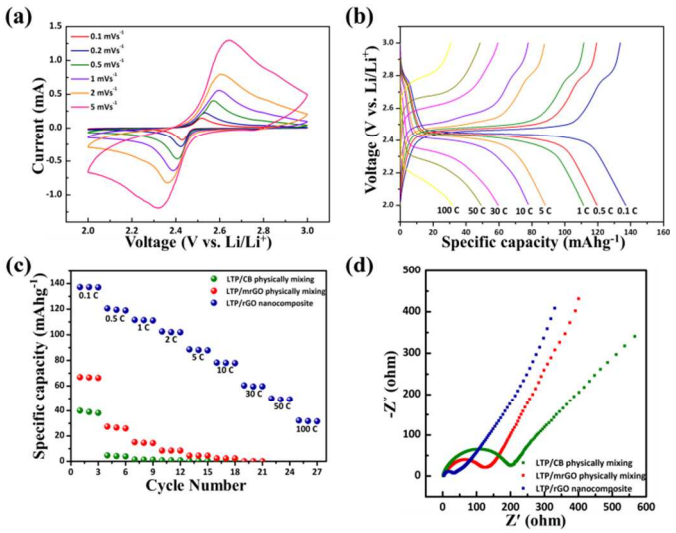

Fig. 3 (a) CV curves for $LiTi_2(PO_4)_3$/rGO electrode at various scanning rates between 2.0 and 3.0 V. (b) The second charge/discharge profiles of the $LiTi_2(PO_4)_3$/rGO electrode at different current rates. (c) Specific discharge capacities at various C-rates. (d) Nyquist plots of $LiTi_2(PO_4)_3$/rGO nanocomposite, $LiTi_2(PO_4)_3$/mrGO, and $LiTi_2(PO_4)_3$/CB materials.

Fig. 3(a) shows peak-shaped cyclic voltammograms (CVs) of the $LiTi_2(PO_4)_3$/rGO nanocomposite measured at increasing potential scan rates from 0.1 to 5 mV s^{-1} in the potential range 2.0–3.0 V (*vs.* Li^+/Li). The cathodic current peak in the CVs corresponds to the reduction of Ti^{4+} to Ti^{3+}, which is responsible for the electrochemical lithiation of the $LiTi_2(PO_4)_3$/rGO electrode, and the anodic current peak corresponds to the oxidation of Ti^{3+} to Ti^{4+}, which is responsible for the electrochemical delithiation process. The CV obtained at 0.1 mV s^{-1} clearly shows a set of well-defined peaks at 2.43 and 2.51 V.[14] Even when the potential scan rate was increased up to 5 mV s^{-1}, the initial shape of the CV was well retained, with little increase in peak potential separation. This suggests facile electrochemical kinetics of the $LiTi_2(PO_4)_3$/rGO electrode.

A linear dependence of the peak current (I_p, peak for the Ti^{4+}/Ti^{3+} redox reaction) on the square root of the scan rate ($\nu^{1/2}$) was observed as shown in Fig. S4.† From this relation, the apparent diffusion coefficient of Li^+ ions in the $LiTi_2(PO_4)_3$/rGO nanocomposite was calculated from the CV data using the Randles-Sevcik equation,

$$I_p/m = 0.4463F(F/RT)^{0.5}A_e(D_{app})^{0.5}C^*_{Li}\nu^{0.5}, \quad (1)$$

as reported previously.[39-45] In Eq. (1), I_p is the peak current (in A), m is the mass of the electrode, F is the Faraday constant (96486 C mol^{-1}), R is the gas constant (8.314 J $mol^{-1}K^{-1}$), T is the absolute temperature (in K), A_e is the electrode area per unit mass (in cm^2 g^{-1}), C^*_{Li} is the initial concentration of Li^+ ions in the $LiTi_2(PO_4)_3$ (0.0076 mol cm^{-3}), ν is scan rate (in V s^{-1}), and D_{app} is the apparent diffusion coefficient (in cm^2 s^{-1}). It should be noted that surface area used in the calculation was for the $LiTi_2(PO_4)_3$ particles after the rGO had been burnt out in air, since only the $LiTi_2(PO_4)_3$ in the $LiTi_2(PO_4)_3$/rGO nanocomposite is electrochemically active in the potential window of 2.0–3.0 V.

From the slope of the linear fit (R-square of 0.999 and 0.987 for anodic and cathodic lines, respectively), the D_{app} values were calculated to be 1.55×10^{-14} and 1.31×10^{-14} cm^2 s^{-1} at 25 °C for the anodic and cathodic reactions, respectively. These obtained values agree well with previously reported results.[46-48]

Fig. 3(b) shows charge/discharge behaviors of the $LiTi_2(PO_4)_3$/rGO nanocomposite obtained between 2.0–3.0 V (*vs.* Li^+/Li) at a C-rate of 0.1 to 100, where each set of charge/discharge tests was performed at the same C-rate. $LiTi_2(PO_4)_3$ in the $LiTi_2(PO_4)_3$/rGO nanocomposite (75 wt.% from thermo-gravimetric analysis as shown in Fig. S5†) shows the specific discharge capacity of 138 mAh g^{-1} based on the weight of $LiTi_2(PO_4)_3$ at 0.1 C-rate. The specific discharge capacity of 49 mAh g^{-1} was achieved even at 50 C-rate, which is 35 % of the 0.1 C-rate specific capacity. The distinct voltage plateaus around 2.48 V are consistent with the CV measurements and correspond to the two-phase reaction that transforms $LiTi_2(PO_4)_3$ to $Li_3Ti_2(PO_4)_3$. Examination of the voltage profiles measured at low C rates, however, clearly shows a short voltage plateau around 2.8 V. Kim's group reported the similar charge curve with a short voltage plateau around 2.8 V, however, with no explanation.[1] Careful examination of the CVs at the potential scan rate of 0.1 mV s^{-1} also shows a small broad hump around 2.8 V during the anodic scan that corresponds to the short voltage plateau around 2.8 V in the charge curves. It has been reported that TiP_2O_7 shows a plateau from the two-phase reaction around 2.6 V *vs.* Li^+/Li upon discharging between $LiTiP_2O_7$ and $Li_{0.8}TiP_2O_7$ with good structural stability during cycling.[49, 50] Though the short potential plateau for the $LiTi_2(PO_4)_3$/rGO nanocomposite is observed at the potential slightly different from that for TiP_2O_7, it is speculated that TiP_2O_7 might be formed during the calcination of the Li–Ti–P–O/rGO intermediate precursor, considering the chemistry used to prepare the composite.

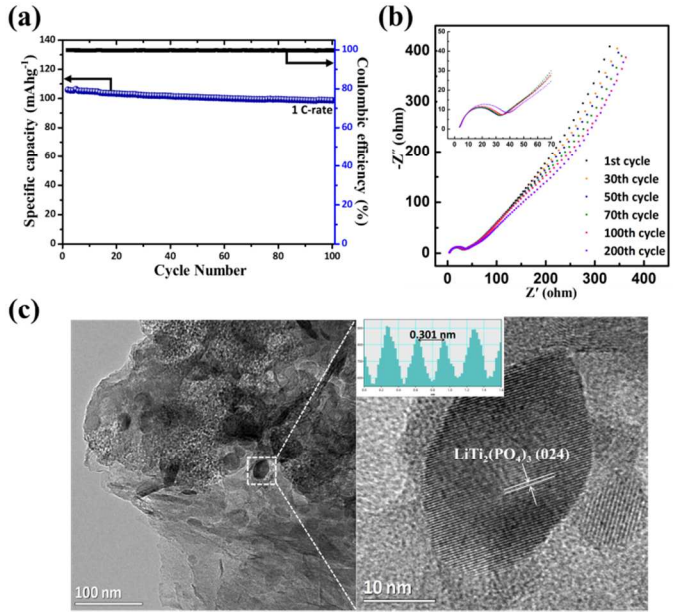

Fig. 4 (a) Cycling stability of the $LiTi_2(PO_4)_3$/rGO electrode material at 1 C-rate. (b) Nyquist plots of $LiTi_2(PO_4)_3$/rGO nanocomposite after 200 cycles at 10 C-rate. (c) TEM and HR-TEM images of the $LiTi_2(PO_4)_3$/rGO nanocomposite demonstrating the coexistence of the relatively unmodified phases of $LiTi_2(PO_4)_3$ nanoparticles, rGO, and residual binder after several charge/discharge cycling.

From the aforementioned XRD analysis, as-synthesized $LiTi_2(PO_4)_3$/rGO nanocomposite is well-matched to the previously reported NASICON-type XRD patterns,[17] however, the absence of diffraction peaks corresponding to TiP_2O_7 compounds suggested from the charge/discharge curves and CVs might be due to the fact that the concentration of TiP_2O_7 was very low in the composite. Its formation during the synthesis of the $LiTi_2(PO_4)_3$/rGO nanocomposite needs further investigation.

The $LiTi_2(PO_4)_3$/rGO nanocomposite shows much improved Li^+ ion storage capacity and rate capability than other electrodes prepared from a physical mixture with an equal amount of conductive carbon. Fig. 3(c) shows the rate performance of the electrode incorporating the $LiTi_2(PO_4)_3$/rGO composite and two other electrodes in which the $LiTi_2(PO_4)_3$ was physically mixed with an equal amount of carbon black (CB) or microwave-reduced graphene oxide (mrGO). The $LiTi_2(PO_4)_3$/rGO composite provides much better rate capability that the others. In particular, the $LiTi_2(PO_4)_3$/rGO nanocomposite retains 56.5 % of its initial capacity at 10 C-rate, whereas capacities of the physically mixed CB and mrGO samples drop dramatically to only 0 % and 3 %, respectively, of the initial capacity at the same rate. This could be attributed to the large effective surface area of the small $LiTi_2(PO_4)_3$ nanoparticles in comparison with that of submicron particles prepared using sol-gel methods (Fig. S6†), which promotes shorter pathways for the solid-state diffusion of lithium ions and intimate contact of the $LiTi_2(PO_4)_3$ nanoparticles and rGO, both of which result in a better rate capability.

In order to verify that the rGO in the $LiTi_2(PO_4)_3$/rGO composite is primarily responsible for the improved electrochemical performance from the view of electrical wiring,[51, 52] electrochemical impedance spectroscopy (EIS) measurements were performed. Fig. 3(d) shows the Nyquist plots of the three different electrodes. The intersection of these curves with the real axis at high frequency is related to the total resistance (R_s) of the electrolyte, active materials, current collectors, and separator. The radius of the semicircle in the middle frequency region typically represents the charge transfer resistance (R_{ct}) at the electrode/electrolyte interface.[53, 54] The $LiTi_2(PO_4)_3$/rGO electrode has the smallest radius with R_{ct} = 36 Ω, whereas the "bare" $LiTi_2(PO_4)_3$ samples mixed with CB (R_{ct} = 205.29 Ω) or mrGO (R_{ct} = 154.462 Ω) showed larger charge transfer resistances. This indicates that an intimate electrical connection between the $LiTi_2(PO_4)_3$ nanoparticles and the rGO template can effectively create more active sites for lithium intercalation/deintercalation and improve the charge transfer reaction, thereby enhancing the rate capability.

The cycling stability of the prepared nanocomposite was also analyzed. Fig. 4(a) shows that the specific capacity of the $LiTi_2(PO_4)_3$/rGO electrode reached 98.76 mAh g^{-1} after 100 cycles at 1 C-rate, a 93.2 % retention of the initial capacity. Furthermore, the coulombic efficiency remained constant at 99.8 % during the repeated cycling, implying excellent electrochemical reversibility and structural stability of the nanocomposite.

To further explore the cycling stability of the nanocomposite, EIS was performed after certain numbers of charge/discharge cycles at 10 C-rate, as shown in Fig. 4(b). After 200 cycles, the charge-transfer resistance of the $LiTi_2(PO_4)_3$/rGO electrode shows little increase, which confirms the good cycling stability of the $LiTi_2(PO_4)_3$/rGO electrode. This suggests both the structural and electrical integrity of the $LiTi_2(PO_4)_3$/rGO composite prepared in this study. To further investigate any structural changes of $LiTi_2(PO_4)_3$ in the $LiTi_2(PO_4)_3$/rGO composite after the repeated cycling, the composite materials in the coin cell were analyzed after 200 cycles by HR-TEM, the results of which are shown in Fig. 4(c). The rectangular area shows clear lattice fringes observed in the HR-TEM image with a d-spacing of 0.301 nm, which corresponds to the (024) plane spacing of $LiTi_2(PO_4)_3$, demonstrating that the high crystallinity of the $LiTi_2(PO_4)_3$ nanoparticles was well retained in the composite during the repeated cycling at 10 C-rate.

Conclusions

An $LiTi_2(PO_4)_3$/reduced graphene oxide (rGO) nanocomposite was prepared using a simple one-pot method, in which an Li–Ti–P–O/rGO precursor was synthesized *in-situ* using a microwave-assisted solvothermal method. Subsequent calcination of the Li–Ti–P–O/rGO precursor yielded a highly crystalline $LiTi_2(PO_4)_3$/rGO nanocomposite, which showed good rate capability and cycling stability. The EIS measurements and post-mortem analysis of $LiTi_2(PO_4)_3$/rGO nanocomposite confirmed the structural and electrical integrity of the $LiTi_2(PO_4)_3$/rGO composite even after 200 cycles at 10 C-rate.

Notes and References

[a] Department of Materials Science & Engineering, Yonsei University, 50 Yonsei-ro, Seodaemun-gu, Seoul 120-749, Republic of Korea. E-mail: kbkim@yonsei.ac.kr
[b] Energy Efficient Materials Team, Energy & Environmental Division, Korea Institute of Ceramic Engineering & Technology, 233-5 Gasan-dong, Guemcheon-gu, Seoul 153-801, Republic of Korea. E-mail: rkc@kicet.re.kr

† Electronic Supplementary Information (ESI) available: One table seven figures showing further details of the properties of the $LiTi_2(PO_4)_3$/rGO nanocomposite. See DOI: 10.1039/b000000x/

1. A. L. M. Reddy, S. R. Gowda, M. M. Shaijumon and P. M. Ajayan, *Adv Mater*, 2012, **24**, 5045-5064.
2. M. Armand and J. M. Tarascon, *Nature*, 2008, **451**, 652-657.
3. J. B. Goodenough and Y. Kim, *Chem Mater*, 2009, **22**, 587-603.
4. B. Kang and G. Ceder, *Nature*, 2009, **458**, 190-193.
5. J. M. Tarascon and M. Armand, *Nature*, 2001, **414**, 359-367.
6. R. Spotnitz and J. Franklin, *Journal of Power Sources*, 2003, **113**, 81-100.
7. M. Yoshio, H. Y. Wang and K. Fukuda, *Angew Chem Int Edit*, 2003, **42**, 4203-4206.
8. M. Yoshio, H. Y. Wang, K. Fukuda, Y. Hara and Y. Adachi, *J Electrochem Soc*, 2000, **147**, 1245-1250.
9. K. S. Kang, Y. S. Meng, J. Breger, C. P. Grey and G. Ceder, *Science*, 2006, **311**, 977-980.
10. K. Amine, I. Belharouak, Z. H. Chen, T. Tran, H. Yumoto, N. Ota, S. T. Myung and Y. K. Sun, *Adv Mater*, 2010, **22**, 3052-3057.
11. J. Y. Luo and Y. Y. Xia, *Adv Funct Mater*, 2007, **17**, 3877-3884.
12. L. Liu, M. Zhou, G. Wang, H. Guo, F. Tian and X. Wang, *Electrochimica Acta*, 2012, **70**, 136-141.
13. V. Aravindan, W. Chuiling and S. Madhavi, *RSC Advances*, 2012, **2**, 7534-7539.
14. V. Aravindan, W. Chuiling, M. V. Reddy, G. V. S. Rao, B. V. R. Chowdari and S. Madhavi, *Physical Chemistry Chemical Physics*, 2012, **14**, 5808-5814.
15. C. Wessells, F. La Mantia, H. Deshazer, R. A. Huggins and Y. Cui, *J Electrochem Soc*, 2011, **158**, A352-A355.
16. T. Jiang, W. Pan, J. Wang, X. Bie, F. Du, Y. Wei, C. Wang and G. Chen, *Electrochimica Acta*, 2010, **55**, 3864-3869.
17. M. Zhou, L. Liu, L. Yi, Z. Yang, S. Mao, Y. Zhou, T. Hu, Y. Yang, B. Shen and X. Wang, *Journal of Power Sources*, 2013, **234**, 292-301.
18. P. Guo, H. H. Song and X. H. Chen, *Electrochem Commun*, 2009, **11**, 1320-1324.
19. A. K. Geim and K. S. Novoselov, *Nat Mater*, 2007, **6**, 183-191.
20. S. Park and R. S. Ruoff, *Nat Nanotechnol*, 2009, **4**, 217-224.
21. C. J. Shih, A. Vijayaraghavan, R. Krishnan, R. Sharma, J. H. Han, M. H. Ham, Z. Jin, S. C. Lin, G. L. C. Paulus, N. F. Reuel, Q. H. Wang, D. Blankschtein and M. S. Strano, *Nat Nanotechnol*, 2011, **6**, 439-445.
22. P. Guo, H. Song, X. Chen, L. Ma, G. Wang and F. Wang, *Analytica Chimica Acta*, 2011, **688,** 146-155.
23. X. J. Zhu, Y. W. Zhu, S. Murali, M. D. Stollers and R. S. Ruoff, *Acs Nano*, 2011, **5**, 3333-3338.
24. Z. S. Wu, G. M. Zhou, L. C. Yin, W. Ren, F. Li and H. M. Cheng, *Nano Energy*, 2012, **1**, 107-131.
25. L. Q. Lu and Y. Wang, *J Mater Chem*, 2011, **21**, 17916-17921.
26. Y. Q. Zou and Y. Wang, *Nanoscale*, 2011, **3**, 2615-2620.
27. S. Q. Chen and Y. Wang, *J Mater Chem*, 2010, **20**, 9735-9739.
28. Y. Q. Zou, J. Kan and Y. Wang, *J Phys Chem C*, 2011, **115**, 20747-20753.
29. J. X. Zhu, T. Zhu, X. Z. Zhou, Y. Y. Zhang, X. W. Lou, X. D. Chen, H. Zhang, H. H. Hng and Q. Y. Yan, *Nanoscale*, 2011, **3**, 1084-1089.
30. C. H. Lim, A. G. Kannan, H.-W. Lee and D. K. Kim, *Journal of Materials Chemistry A*, 2013, **1**, 6183-6190.
31. W. S. Hummers and R. E. Offeman, *Journal of the American Chemical Society*, 1958, **80**, 1339-1339.
32. C. R. Mariappan, C. Galven, M. P. Crosnier-Lopez, F. Le Berre and O. Bohnke, *Journal of Solid State Chemistry*, 2006, **179**, 450-456.
33. H. M. A. Hassan, V. Abdelsayed, A. E. R. S. Khder, K. M. AbouZeid, J. Terner, M. S. El-Shall, S. I. Al-Resayes and A. A. El-Azhary, *Journal of Materials Chemistry*, 2009, **19**, 3832-3837.
34. A. V. Murugan, T. Muraliganth and A. Manthiram, *Chem Mater*, 2009, **21**, 5004-5006.
35. D. Chen, K. B. Tang, G. Z. Shen, J. Sheng, Z. Fang, X. M. Liu, H. G. Zheng and Y. T. Qian, *Mater Chem Phys*, 2003, **82**, 206-209.
36. S. Baek, S. H. Yu, S. K. Park, A. Pucci, C. Marichy, D. C. Lee, Y. E. Sung, Y. Piao and N. Pinna, *RSC Advances*, 2011, **1**, 1687-1690.
37. H. K. Kim, J. P. Jegal, J. Y. Kim, S. B. Yoon, K. C. Roh and K. B. Kim, *Journal of Materials Chemistry A*, 2013, **1**, 14849-14852.
38. H. K. Kim, K. C. Roh, K. Kang and K. B. Kim, *RSC Advances*, 2013, **3**, 14267-14272.
39. A. V. Churikov, A. V. Ivanishchev, I. A. Ivanishcheva, K. V. Zapsis, I. M. Gamayunova and V. O. Sycheva, *Russ J Electrochem*, 2008, **44**, 530-542.
40. A. Ivanishchev, A. Churikov and A. Ushakov, *Electrochimica Acta*, 2014, **122**, 187-196.
41. M. Levi, G. Salitra, B. Markovsky, H. Teller, D. Aurbach, U. Heider and L. Heider, *J Electrochem Soc*, 1999, **146**, 1279-1289.
42. X. H. Rui, N. Ding, J. Liu, C. Li and C. H. Chen, *Electrochimica Acta*, 2010, **55**, 2384-2390.
43. J. Xie, N. Imanishi, T. Matsumura, A. Hirano, Y. Takeda and O. Yamamoto, *Solid State Ionics*, 2008, **179**, 362-370.
44. S. B. Tang, M. O. Lai and L. Lu, *Mater Chem Phys*, 2008, **111**, 149-153.
45. J. Come, P. L. Taberna, S. Hamelet, C. Masquelier and P. Simon, *J Electrochem Soc*, 2011, **158**, A1090-A1093.
46. P. P. Prosini, M. Lisi, D. Zane and M. Pasquali, *Solid State Ionics*, 2002, **148**, 45-51.
47. F. Gao and Z. Y. Tang, *Electrochimica Acta*, 2008, **53**, 5071-5075.
48. G. X. Wang, D. H. Bradhurst, S. X. Dou and H. K. Liu, *Journal of Power Sources*, 2003, **124**, 231-236.
49. V. Aravindan, M. V. Reddy, S. Madhavi, S. G. Mhaisalkar, G. V. S. Rao and B. V. R. Chowdari, *Journal of Power Sources*, 2011, **196**, 8850-8854.
50. S. Patoux and C. Masquelier, *Chem Mater*, 2002, **14**, 5057-5068.
51. S. B. Yoon, H. K. Song, K. C. Roh and K. B. Kim, *J Electrochem Soc*, 2014, **161**, A137.
52. S. B. Yoon, J. P. Jegal, K. C. Roh and K. B. Kim, *J Electrochem Soc*, 2014, **161**, H207.
53. K. Dokko, M. Mohamedi, M. Umeda and I. Uchida, *J Electrochem Soc*, 2003, **150**, A425-A429.

54. Y. Shi, L. Wen, F. Li and H.-M. Cheng, *Journal of Power Sources*, 2011, **196**, 8610-8617.